

# Computation of couple stress electroconductive polymer from an exponentially stretching sheet

J.C. Umavathi<sup>a,\*</sup>, M. Sankar<sup>b</sup>, O.Anwar Bég<sup>c</sup>, Ali J. Chamkha<sup>d</sup>

<sup>a</sup> Professor, Department of Mathematics, Gulbarga University, Gulbarga-585 106, Karnataka, India

<sup>b</sup> Department of General Requirements, University of Technology and Applied Sciences - Ibra, P.O. Box 14, Ibra 516, Oman

<sup>c</sup> Professor of Engineering Science, Aeronautical & Mechanical Engineering Department, School of Science, Engineering and Environment, Newton Building, University of Salford, Manchester M54WT, UK

<sup>d</sup> Faculty of Engineering, Kuwait College of Science and Technology, Doha District, 35004 Kuwait

## ARTICLE INFO

### Keywords:

Magnetic polymers  
Rheology  
Polar couple stress model  
Hall current  
Ohmic dissipation  
Viscous heating  
Exponential stretching  
Heat transfer  
Primary and secondary flow  
MATLAB

## ABSTRACT

Magnetic polymer processing involves multiple physical phenomena and requires simultaneous consideration of rheological, hydromagnetic and thermal characteristics. Inspired by new developments in functional magnetic coating dynamics, the present article investigates the viscous magnetohydrodynamic non-Newtonian boundary layer flow of an incompressible, electrically conducting, couple stress, electroconductive polymer from an exponentially stretching sheet. The nonlinear boundary value problem is solved numerically by adopting shooting technique and *bvp4c* algorithm available in MATLAB software. Validation with the Adams-Moulton 2-step predictor corrector algorithm is included. The effects of non-Newtonian couple stress parameter, magnetic interaction number, mixed convection parameter, slip parameter, Prandtl and Eckert number on the primary and secondary velocities and temperature fields are visualized graphically. Greater hydrodynamic slip effect initially boosts the primary velocity near the wall but thereafter induces a decrement in it. However, a consistent improvement in secondary velocity is computed for greater slip parameter. Increasing Hall parameter strongly accelerates the secondary flow but only weakly accelerates the primary flow. Increasing magnetic interaction number decelerates the primary and secondary flow. Elevating magnetic number promotes the thermal boundary layer thickness and also the temperature. Couple stress effects generally accelerate both the primary and secondary flow.

## 1. Introduction

During the past few years, many polymeric materials have become smart, capable of responding to multiple stimuli in the field, with multiple levels of intelligence. In polymer-based composite materials called electro/magneto-active polymers (E/MAPs), these complex multifunctional materials are capable of adapting their behavior to alternating electrical or magnetic fields. The fillers of these materials are generally soft polymer matrixes with magnetic particles inside them [1,2]. It has been reported that such materials are capable of integrated multifunctionality in several studies, including [3]. This type of material can also be found in electromagnetic shape memory polymers (for robotics and medical coatings that soften through magnetic induction) [4], electro-polymers with integrated shape memory [5,6], ferroelectric polymers with smart hydrogels and electro-active polymers with programmable

\* Corresponding author.

E-mail address: [drumavathi@rediffmail.com](mailto:drumavathi@rediffmail.com) (J.C. Umavathi).

**Nomenclature**

$B$	magnetic field vector
$B_0$	constant magnetic field
$C$	couple stress parameter
$c_p$	specific heat at constant pressure
$Cf_x$	local skin friction coefficient
$E$	electrical field vector
$Ec$	Eckert number
$f$	dimensionless primary stream function
$G$	dimensionless secondary (cross flow) velocity
$Gr_x$	local Grashof number
$K$	rheological consistency co-efficient
$k$	thermal conductivity of fluid
$L$	characteristic length
$m$	Hall current parameter
$M$	magnetic parameter
$Nu_x$	local Nusselt number
$Pr$	generalized Prandtl number
$Re$	local Reynolds number
$Re_x$	generalized local Reynolds number
$T$	fluid temperature
$T_w$	temperature at the wall
$T_\infty$	ambient temperature of the fluid
$u$	velocity component in the $x$ -direction
$U_0$	characteristic velocity
$u_w$	stretching sheet velocity
$v$	velocity component in the $y$ -direction
$w$	velocity component in the $z$ -direction
$x$	stream wise coordinate
$y$	cross-stream (transverse) coordinate

**Greek symbols**

$\alpha$	thermal diffusivity
$\beta$	volumetric coefficient of the thermal expansion
$\delta$	mixed convection parameter
$\theta$	dimensionless temperature
$\rho$	fluid density
$\eta$	similarity independent variable
$\lambda$	generalized slip parameter
$\lambda^*$	primary hydrodynamic slip coefficient
$\lambda_1$	secondary hydrodynamic slip coefficient
$\xi$	mixed convection parameter
$\tau_w$	primary wall shear stress
$\psi$	stream function
$\Omega$	dimensionless temperature difference

**Subscripts**

$w$	quantities at wall
$\infty$	quantities far away from the surface

electrostatic properties [7]. Such rheological models depart considerably from the classical Navier-Stokes viscous flow mode and include an extensive range of formulations. Furthermore, no single model is claimed to encompass all possible features (e. g. shear thinning/thickening, viscoelastic stress relaxation, viscoplastic yield flow, material retardation, spurting effects, etc.). A complex boundary condition, nonlinearity in the governing equations, and coupling are the challenges of these problems. Mathematicians, engineers, and polymer physicists who work with micron-sized suspended particles (such as magnetic functional particles) are particularly attracted to these problems.

There is a wide variety of mathematical models for suspensions according to their concentration and size in the available literature. Excellent treatises on non-Newtonian fluid dynamics reviewing multiple models e. g. Sisko, Bingham plastic, Oldroyd B, Williamson fluids, etc. have been provided by Bird *et al.* [8] and Shaw [9]. Despite the popularity of non-Newtonian models described in [8,9], they

do not offer any details on the microstructure of rheological fluids e. g. polymers. In the 1960s therefore a new generation of non-Newtonian models emerged in which microstructure was incorporated in the field equations. The most elegant of these formulations is the Eringen micromorphic framework [10] which for the first time generalized all angular motions and axial contractions/extensions of particles suspended (“microelements”) in rheological media. Special cases of these microfluids were termed micropolar fluids [11] and microstretch fluids [12]. A much simpler model that can be retrievable from the Eringen micropolar model is the *Stokes polar couple-stress theory model* [13].

According to this model, the microelements’ spin must match the vorticity of the carrier fluid. According to Stokes [14] and Eringen [10] several theories of fluid micro-continua have been developed by taking into account couple stresses. Couple-stress fluids, which are classified as non-Newtonian fluids, are characterized by polar effects and high viscosities. In an anti-symmetric stress field, free particles creating an anti-symmetric spin field set up anti-symmetric stress, resulting in a couple-stress fluid. The couple stress fluid theory is predicated on the idea that couple stresses exist but that the fluid lacks any microstructure at the kinematic level and that the velocity field alone dictates the kinematics of motion, according to Stokes [14] In reality, a couple stress fluid can be described by two parameters: one for couple stresses and the other for viscosity in the Newtonian fluid.

Many interesting studies of couple stress fluid dynamics have been communicated. A great assessment of the viability of couple stress fluid dynamics in chemical and mechanical engineering has been given by Cowin [15]. Mokhiamer et al. [16] studied elasto-hydrodynamic tribological flows with the couple stress model. Devakar et al. [17] studied the slip on the boundaries on the generalized Couette and Poiseuille flows of couple stress fluid in channels. Devakar and Iyengar [18] discussed the flow between moving plates filled with coupled stress fluid. Islam et al. [19] explored the Poiseuille and Couette flow for the couple stress fluid. Heat transfer of couple stress Poiseuille flow was computed by Farooq et al. [20]. Soundalgekar et al. [21] investigated Taylor dispersion and couple stress effects in mass transfer in a channel. Zueeo and Bég [22] used PSPICE electrothermal software to compute the periodic flow of blood with a combined polar and Eyring-Powell model, noting that stronger couple stresses accelerate the flow. Further studies include Umavathi et al. [23] on thermo-convection of couple stress fluid, Srinivasacharya and Srikanth [24] (on couple stress hydrodynamic in a narrow annular geometry), Ogulu [25] (couple stress fluid on boundary layer flow) Malshetty et al. [26] (on Oberbeck convection in a vertical porous channel), Umavathi et al. [27] (on couple stress flow in a horizontal stratum). Recently Kumar et al. [28] used the DTM to simulate transient stretching flow and convective heat transfer from a coupled stress coating on a stretching sheet. Umavathi and Bég [29] researched on the hydrodynamic and thermal stability of a couple of stress nanofluid containing nanoparticles.

The first-order uniform chemical reaction of a viscous incompressible unsteady flow of fluid passing on an oscillatory infinite long vertical plate was studied by Awan *et al.* [30] with modified temperature and uniform mass diffusivity. They concluded that the velocity of the fluid increased with a decrease in phase angle, while it increased with chemical reaction parameters and time. Awan et al. [31] studied the longitudinal flow of a fractional Maxwell fluid between two infinite coaxial circular cylinders with Laplace and finite Hankel transforms. They found that the fractional parameter reduces the velocity but increases the shear stress. Awan et al. [32] analyzed the time-independent performance of two-dimensional non-Newtonian nanofluid flow on a circular stretching cylinder. They noted that flow acceleration is induced with increasing curvature values and Sutterby nanofluid parameters whereas it is suppressed with magnetic, thermophoresis, stretching and Darcy resistance parameters. Third-grade micropolar fluid flow over an exponentially stretched surface was investigated by Guedri et al. [33]., in which it was found that the concentration distribution diminishes with higher values of Brownian motion number and Lewis number but is enhanced with the thermophoresis parameter. Ali et al. [34]. analyzed the significance of linear and quadratic convection in the rotating flow of a micropolar fluid due to a stretching surface in the presence of magnetic force. They found that the velocity profile decreased with a boost in magnetic and rotating parameters and fluid velocity was higher in the nonlinear (quadratic) convection case. A Mixed convection flow of fractional Maxwell fluid was scrutinized by Awan et al. [35]. under the impact of pressure gradient and it was observed that the velocity characteristics are strongly modified with an increment in Péclet and Reynolds numbers in addition to time. Awan et al. [36]. analyzed heat transferrin unsteady oblique stagnation point flow of an incompressible second-grade fluid on a stretching surface with some slip effects, noting that an increment in the local second-grade parameter depletes Sherwood number whereas the Nusselt values are enhanced by decreasing the local second-grade parameter. Hydromagnetic free convection in incompressible viscous fluid flow with generalized boundary conditions was studied by Ali et al. [37]. They reported that the velocity was increased with higher values of fractional factors and the boundary layer thickness boosted with time elapse. Awan et al. [38]. investigated numerically the Ellis hybrid nanofluid flow model with magnetic, Darcy-Forchheimer, and non-linear thermal radiation effects across the stretching cylinder. They found that velocity magnitudes of unitary and hybrid nanofluids declined for higher inputs of Darcy–Forchheimer and magnetic parameters whereas temperatures were enhanced with thermal radiation and thermal Biot numbers. Non-Newtonian blood flows through a multi-stenosed artery of the elliptical cross-section was analyzed by Shahzad et al. [39]. They observed that the non-Newtonian fluid achieves lower velocities than the Newtonian fluid and a strong deviation in wall shear stress is computed for these two cases. Abbas et al. [40]. applied a power law nanofluid model to simulate transport from a stretching Riga electromagnetic sensor surface. They noted that a strong enhancement in variable thermal conductivity parameter, thermophoresis parameter, Eckert number, and heat generation parameter causes a significant rise in the temperature profiles, while the opposite trend is computed for higher Prandtl numbers. Shatnawi et al. [41]. examined the steady flow of an incompressible hybrid Casson nanofluid over a vertical permeable exponential stretching sheet, showing that the Yamada-Ota model achieved a higher heat transfer rate than the Xue and Tiwari Das models for hybrid nanofluids. Heat and mass transfer study of hybrid nanomaterial Casson fluid in unsteady stagnation flow over a vertical Riga sheet was addressed by Shatnawi et al. [42]. who showed that the electric forces increase due to higher values of the modified Hartmann number, ultimately reducing velocity magnitudes.

The first experimental investigation in MHD flow (as reviewed in Bég et al. [43]) was conducted by Hartmann and Lazarus [44] who determined the effects of electric and magnetic fields on incompressible viscous flow in a channel (duct) comprising parallel

plates. This provided a modern base for MHD studies. A key area in modern magnetic materials is smart polymer processing. The seminal paper initiating Newtonian flow on a stretching surface was presented by Crane [45] in which similar solutions were derived. This work has been extensively refined for more complex magnetohydrodynamic flows and also with multiple physics effects in recent years, largely fueled by the emergence of many new coating materials featuring functionality. Stretching enables homogenous coatings to be synthesized on a range of geometries in engineering including horizontal substrates, gas turbine blades, solar photovoltaic collector receivers, medical devices, etc. External magnetic fields have been shown both theoretically and practically to achieve excellent non-intrusive flow control in electromagnetic materials processing systems. Akbaret al. [46] investigated magnetic nanofluid boundary layer flow from a vertical stretching sheet. These studies were however confined to linear stretching of the sheet. More complex stretching scenarios also arise in magnetic materials processing including quadratic stretching [47], cubic velocity power-law stretching [48] and exponential stretching [49]. Magnetohydrodynamic flows of coupled stress fluids have also received some attention. Nayak and Dash [50] investigated Lorentzian drag effects in rotating hydromagnetic couple stress channel flow in Darcian permeable media. Ramesh and Davekar [51] investigated the bioinspired pumping of hydromagnetic couple stress flow, in a vertical conduit containing a porous media. These studies showed that couple stress effects induce significant deviation from Newtonian flows and magnetic fields generally decelerate the flow whereas they elevate thermal and mass diffusion rates.

The above investigations were generally confined to *no-slip* boundary condition scenarios. However polymeric flows are often associated with slippery interface behavior. This leads to *non-compliance* with the polymer with the boundary. The classical no-slip wall condition is not adequate for simulating such flows where fluid slippage is significant. In the 19th century, Navier established a generic boundary condition that allows for slide at the solid boundary. Several experiments have confirmed the presence of slip in real polymer flows, including Piau and Kissi [52] (on polymer melts), Piau et al. [53] (on polymer extrudate distortion), Wang and Drda [54] (on polyethylene melts). Several theoretical studies of magnetic polymer flow with wall slip have been communicated. Bhatti et al. [55] with the help of a successive Taylor algorithm solved the hydrodynamic and thermal slip effects in cross-diffusion ferrite magnetic nanofluid flow. Béget al. [56] adopted PSPICE electrothermal software to understand slip effects of magnetic polymers. In polymer thermal processing which features shear flows, non-viscometric behavior and boundary layer growth, *viscous heating* is also known to arise. Several investigators have also addressed therefore the influence of viscous heating in magnetohydrodynamics. Furthermore, magnetic fields may also generate Joule heating or Ohmic dissipation. Both effects are known to heat the working fluid and induce deceleration. Mishra et al. [57] considered the variation parameter method to determine the thermal relaxation impact in tribological squeezing hydromagnetic flow in a Riga sensor system with viscous and Ohmic dissipation. Viscous and Joule heating effects in thermo-magnetic, coupled stress nanofluid boundary layer flow along a linearly stretching sheet were studied by Kumar et al. [58].

In the present study, we generalize the earlier models of [59,60] to consider hydrodynamic slip and couple stress rheology of magnetic polymers. A mathematical model is therefore developed for viscous magnetohydrodynamic boundary layer flow of an incompressible, electrically conducting, polar (couple stress) electroconductive polymer from an exponentially stretching sheet. Owing to slippery motion at the substrate, a slip velocity is included. A secondary flow is induced with the presence of a Hall current, which has also been demonstrated to have a major impact on the processing of magnetic materials, as defined by Bhatti et al. [61]. Ohmic and viscous dissipations are also incorporated in the mathematical formulation. The nonlinear boundary value problem is solved by adopting shooting technique and bvp4c algorithm available in MATLAB software. Validation with the Adams-Molton 2-step predictorcorrector algorithm is included. The effects of non-Newtonian couple stress parameter, magnetic interaction number, mixed convection parameter, slip parameter, Prandtl and Eckert number on the primary and secondary velocities and temperature fields are visualized graphically. Primary and secondary shear stress components and Nusselt number at the substrate are also computed. The

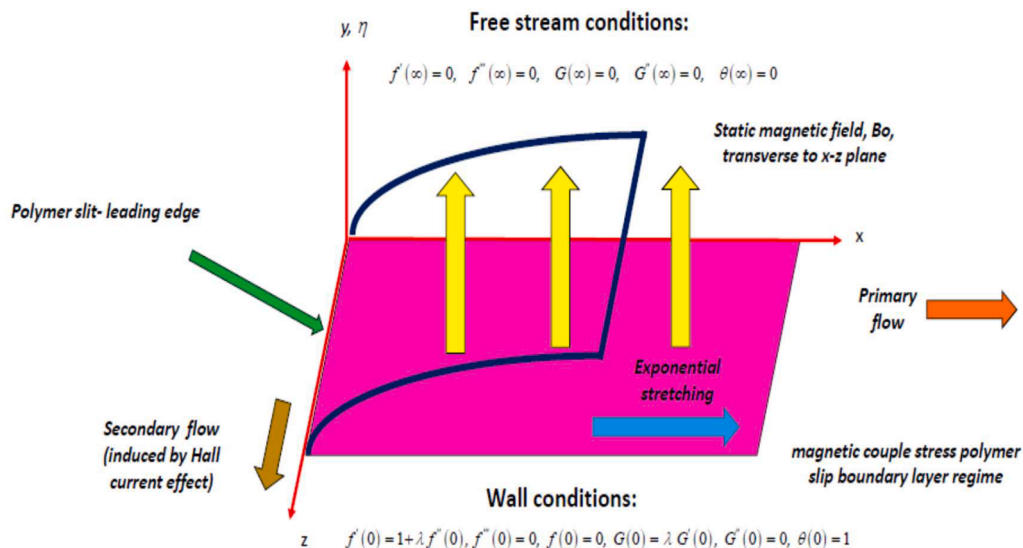


Fig. 1. Exponential sheet stretching of an electroconductive polymer.

uniqueness of this investigation is the unique combination of couple stress (polymer rheology), Hall current and hydrodynamic slip effects, which have thus far not been simultaneously studied in magnetic polymer boundary layer coating flows.

## 2. Mathematical model

An  $(x, y, z)$  coordinate system is used to model heat transfer in an incompressible, constant hydromagnetic boundary layer flow of an electroconductive polymer from an exponentially stretching sheet. Perpendicular to the sheet’s surface, a static magnetic field  $B_0 e^{x/2L}$  is applied. Electrical polarization voltage is neglected, and magnetic Reynolds number is low enough to counteract the influence of magnetic induction. However, Hall current is considered which generates a secondary flow. To simulate dissipation effects encountered in polymers, both viscous heating and Ohmic dissipation (Joule magnetic heating) are included. Stokes’s couple stress model is adopted to represent the magnetic polymer. Magnetic polymer issues from a slit at  $x = 0$  (leading edge) and the boundary layer coating grows with  $x$  coordinate, as shown in Fig. 1. The velocity in the  $x$ -direction is assumed as  $U_w(x) = U_0 e^{x/L}$  where  $U_0$  is the reference velocity,  $L$  a characteristic length. The polymer has ambient temperature  $T_\infty$ . The polar couple stress model introduces extra couple stresses in the Navier-Stokes equations, via the *biharmonic operator* ( $\nabla^4 = \nabla^2 \cdot \nabla^2$ ). Furthermore, both main and secondary momentum equations will include the couple stress fluid constant. The ratio of  $\eta$  and  $\mu$  is considered as  $l^2 (= \eta/\mu)$  as defined in the couple stress fluid theory [13,14,15].

Therefore, Stokes couple stress fluid theory [13] defines the stress tensors related to couple stresses as follows:

$$\tau_{ij} = (-P + \lambda \nabla \cdot U) \delta_{ij} + 2\mu d_{ij} - \frac{1}{2} \varepsilon_{ijk} (m_{ij} + 4\eta \omega_{k,rr} + \rho c_k), \tag{1}$$

$$m_{ij} = \frac{1}{3} m \delta_{ij} + 4\eta' \omega_{i,j}. \tag{2}$$

Here  $\omega = \frac{1}{2} (\nabla \times U)$ ,  $m = m_{11} + m_{22} + m_{33}$  and  $\omega_{k,rr} = \omega_{k,11} + \omega_{k,22} + \omega_{k,33}$ .

In Eqns. (1) and (2),  $\tau_{ij}$  represents the force-related stress tensor,  $m_{ij}$  is the couple stress tensor,  $\omega_{i,j}$  is the tensor related to spin (i.e.,  $\omega = \frac{1}{2(\nabla \times \nabla)}$ ),  $d_{ij}$  is rate of deformation tensor  $d_{ij} = \frac{1}{2(\nabla_{i,j} + \nabla_{j,i})}$ , operator of Kronecker delta is  $\delta_{ij}$ , vector of the velocity is  $U$ , symbol of Levi-Civita is  $\varepsilon_{ijk}$ , the spin vector is  $\omega$  and vector of the body couple is  $\rho c_k$ . The coefficients of viscosity are  $\mu$  and  $\lambda$  and they are expressed as follows in terms of  $\eta$  and  $\eta'$  which are the couple stress coefficients of viscosity.

$$\mu \geq 0, 2\mu + 3\lambda \geq 0, \eta \geq 0 \text{ and } |\eta'| \leq \eta. \tag{3}$$

Since the polymer is electrically conducting, MHD effects are invoked. [30] provides the following

$$j + \frac{\omega_e \tau_e}{B} (j \times B) = \sigma (E + V \times B). \tag{4}$$

Here  $V = (u, 0, w)$  (velocity),  $B = (0, B_0, 0)$  (magnetic field),  $j = (j_x, j_y, j_z)$  (current density),  $\sigma$  (electric conductivity),  $\omega_e$  (frequency of the cyclotron) and  $\tau_e$  (time taken for the electron collision). Primary and secondary current density components are:

$$j_x - m j_z = -\sigma w B_0, \quad j_z + m j_x = \sigma u B_0, \tag{5}$$

where  $m = \omega_e \tau_e$  (Hall parameter). Further  $j_x$  and  $j_z$  take the form as

$$j_x = \frac{\sigma B_0}{1 + m^2} (mu - w), \quad j_z = \frac{\sigma B_0}{1 + m^2} (u + mw). \tag{6}$$

Following Das et al. [59] and Shamsuddin et al. [60] the balance laws are

$$\frac{\partial u}{\partial x} + \frac{\partial v}{\partial y} = 0, \tag{7}$$

$$u \frac{\partial u}{\partial x} + v \frac{\partial u}{\partial y} = -\frac{\eta_0}{\rho} \left( \frac{\partial^4 u}{\partial y^4} \right) + g \beta_T (T - T_\infty) - \frac{\sigma B_0^2}{\rho (1 + m^2)} (u + mw), \tag{8}$$

$$u \frac{\partial w}{\partial x} + v \frac{\partial w}{\partial y} = -\frac{\eta_0}{\rho} \left( \frac{\partial^4 w}{\partial y^4} \right) + \frac{\sigma B_0^2}{\rho (1 + m^2)} (mu - w), \tag{9}$$

$$u \frac{\partial T}{\partial x} + v \frac{\partial T}{\partial y} = \alpha \frac{\partial^2 T}{\partial y^2} + \frac{\sigma B_0^2}{\rho c_p} (u^2 + w^2) + \frac{K}{\rho c_p} \left[ \left( \frac{\partial u}{\partial y} \right)^2 + \left( \frac{\partial w}{\partial y} \right)^2 \right]. \tag{10}$$

The relevant conditions are

At  $y = 0$ :

$$u = u_w(x) + \lambda^* \frac{\partial u}{\partial y}, \quad \frac{\partial^2 u}{\partial y^2} = 0, \quad v = 0, \quad w = \lambda^* \frac{\partial w}{\partial y}, \quad \frac{\partial^2 w}{\partial y^2} = 0, \quad T = T_\infty + T_0 e^{x/2L}. \tag{11}$$

As  $y \rightarrow \infty$ :

$$u \rightarrow 0, \quad \frac{\partial^2 u}{\partial y^2} \rightarrow 0, \quad w \rightarrow 0, \quad \frac{\partial^2 w}{\partial y^2} \rightarrow 0, \quad T \rightarrow T_\infty. \tag{12}$$

The continuity equation is satisfied by introducing a stream function  $\psi(x, y)$  defined in the usual form  $u = \frac{\partial \psi}{\partial y}$ ,  $v = -\frac{\partial \psi}{\partial x}$ . In order to convert the momentum and energy Eqs. (5-7) to ordinary differential equations, the following similarity variables are utilized.

$$\psi = \sqrt{\frac{2KL U_0}{\rho}} e^{x/2L} f(\eta), \quad u = U_0 e^{x/L} f'(\eta), \quad v = -\sqrt{\frac{2KL U_0}{\rho L}} e^{x/2L} \frac{1}{2} [f(\eta) + \eta f'(\eta)], \quad w = U_0 e^{x/L} G(\eta), \quad \theta = \frac{T - T_\infty}{T_w - T_\infty},$$

$$\eta = y \sqrt{\frac{\rho U_0}{2KL}} e^{x/2L}. \tag{13}$$

Substitution of Eqn. (9) into Eqns. (5-7) leads to the following system of coupled, nonlinear ordinary differential equations:

**Primary momentum**

$$\frac{C Re_x}{4} f^{\prime\prime\prime} + (f')^2 - \frac{f f''}{2} - \delta \theta + \frac{M}{(1 + m^2)} (f' + mG) = 0, \tag{14}$$

**Secondary momentum**

$$\frac{C Re_x}{4} g^{\prime\prime\prime} + fG - \frac{f G'}{2} - \delta \theta - \frac{M}{(1 + m^2)} (m f' - G) = 0, \tag{15}$$

**Energy**

$$\theta'' + Pr Ec M ((f')^2 + G^2) + \frac{Pr Ec}{2} (f'' + (G')^2) + \frac{Pr}{2} f \theta' = 0. \tag{16}$$

The following emerges as the boundary conditions at the surface (substrate) and at the boundary layer's edge (free stream):

$$f'(0) = 1 + \lambda f''(0), \quad f''(0) = 0, \quad f(0) = 0, \quad G(0) = \lambda G'(0), \quad G'(0) = 0, \quad \theta(0) = 1,$$

$$f'(\infty) = 0, \quad f''(\infty) = 0, \quad G(\infty) = 0, \quad G'(\infty) = 0, \quad \theta(\infty) = 0. \tag{17}$$

$$C = \frac{\eta_0}{K L^2}, \quad M = \frac{\sigma B_0^2 L}{\rho u_w(x)}, \quad Re = \frac{\rho L u_w(x)}{K}, \quad Gr_x = \frac{g \beta_T (T_w - T_\infty) L^3 \rho^2}{K^2}, \quad \delta = \frac{Gr_x}{Re^2},$$

$$Re_x = \frac{\rho u_w L}{K}, \quad \alpha = \frac{K}{\rho c_p}, \quad Pr = \frac{2K}{\alpha \rho}, \quad Ec = \frac{u_w^2}{(T_w - T_\infty) c_p}. \tag{18}$$

where  $M$  denotes the magnetic,  $\delta$ , the mixed convection,  $Pr$ , Prandtl number,  $Ec$ , Eckert number and  $\lambda$ , slip parameters.

The skin friction coefficient (primary and secondary), and Nusselt numbers are the physical quantities of relevance in materials processing engineering and can be calculated using the following expressions:

$$\tau_{wx} = \left( K \frac{\partial u}{\partial y} \right)_{y=0} = \frac{K u_w}{L} \sqrt{\left( \frac{Re_x}{2} \right)} f'(0). \tag{19}$$

$$Cf_x = \frac{2 \tau_w}{\rho u_w^2} = \sqrt{\frac{Re_x}{2}} f'(0). \tag{20}$$

$$\tau_{wz} = \left( K \frac{\partial w}{\partial y} \right)_{y=0} = \frac{K u_w}{L} \sqrt{\left( \frac{Re_x}{2} \right)} g'(0). \tag{21}$$

$$Cf_z = \frac{2 \tau_w}{\rho u_w^2} = \sqrt{\frac{Re_x}{2}} g'(0). \tag{22}$$

$$Nu_x = - \frac{L}{T_w - T_\infty} \left( \frac{\partial T}{\partial y} \right)_{y=0} = - \sqrt{\frac{Re_x}{2}} \theta'(0). \tag{23}$$

### 3. Matlab quadrature numerical solutions

Closed form solutions can not be found for the Eqs. (14)-(16) as they are nonlinear. Hence the approximate solutions are found numerically using shooting method. By making the following assumptions, the higher order system is reduced to a system of several first order equations:

$$\begin{aligned} y_1 &= f, y_2 = f', y_3 = f'', y_4 = f''', y_5 = f^{iv}, y_6 = g, y_7 = g', \\ y_8 &= g, y_9 = g', y_{10} = \theta, y_{11} = \theta'. \end{aligned} \tag{24}$$

$$y_5' = \frac{4}{C Re_x} \left[ -y_2^2 + \frac{y_1 y_3}{2} + \delta y_{10} - \frac{M}{1+m^2} (y_2 + m y_6) \right], \tag{25}$$

$$y_9' = \frac{4}{C Re_x} \left[ -y_2 y_6 + \frac{y_1 y_7}{2} + \frac{M}{1+m^2} (m y_2 - y_6) \right], \tag{26}$$

$$y_{11}' = -M Pr Ec [y_2^2 + y_6^2] - \frac{Pr Ec}{2} [y_3^2 + y_7^2] - \frac{Pr y_1 y_{11}}{2}. \tag{27}$$

The associated border values become:

$$\begin{aligned} y_1(0) &= 0, y_2(0) = 1 + \lambda y_3(0), y_4(0) = 0, y_6(0) = \lambda g_7(0), y_8(0) = 0, y_{10}(0) = 1, \\ y_2(\infty) &= 0, y_4(\infty) = 0, y_6(\infty) = 0, y_8(\infty) = 0, y_{10}(\infty) = 0. \end{aligned} \tag{28}$$

The iterations are carried out up to the order of  $10^{-6}$ .

### 4. Validation with adams-moulton 2-Step predictor-corrector scheme

The BVP4C finite difference results cannot be compared to complete solutions because the current model is unique. An alternative numerical technique, the Adams Moulton predictor-corrector approach, is therefore used to validate the computations. In depth information is provided in Bég [62], Bég et al. [63] and Pal [64]. Instead of turning off innovative features to return to earlier models from the literature, this verification approach has the important advantage that the entire model created in the present work may be confirmed, i. e. with all effects included. The implicit multistep approach used by Adams Moulton is one. For a linear initial value issue, the rapidly convergent, stable, two-step Adams Moulton approach is a well-liked variant. When this algorithm is used to solve the current boundary value problem, we specify the  $f, g$  and  $h$  as

$$\left. \begin{aligned} \frac{df}{d\eta} &= v(\eta, f), f(\eta_0) = f_0 \\ \frac{dg}{d\eta} &= v(\eta, \theta), g(\eta_0) = g_0 \\ \frac{dh}{d\eta} &= v(\eta, \theta), h(\eta_0) = h_0. \end{aligned} \right\} \tag{29}$$

Here  $f_0, g_0, h_0$  are initial guesses. The four variables' Adams-Moulton two-step predictor relations with a stepping distance of  $\zeta$  have the following form:

$$\left. \begin{aligned} f_{k+1} &= f_k + \frac{\zeta}{2} (3v(\eta_k, f_k) - v(\eta_{k-1}, f_{k-1})) \\ g_{k+1} &= g_k + \frac{\zeta}{2} (3v(\eta_k, g_k) - v(\eta_{k-1}, g_{k-1})) \\ h_{k+1} &= h_k + \frac{\zeta}{2} (3v(\eta_k, h_k) - v(\eta_{k-1}, h_{k-1})). \end{aligned} \right\} \tag{30}$$

The two-step corrector formulas are provided by:

$$\left. \begin{aligned} f_{k+1} &= f_k + \frac{\zeta}{2} (v(\eta_{k+1}, f_{k+1}) - v(\eta_k, f_k)) \\ g_{k+1} &= g_k + \frac{\zeta}{2} (v(\eta_{k+1}, g_{k+1}) - v(\eta_k, g_k)) \\ h_{k+1} &= h_k + \frac{\zeta}{2} (v(\eta_{k+1}, h_{k+1}) - v(\eta_k, h_k)). \end{aligned} \right\} \tag{31}$$

To verify the MATLAB BVP4C solutions, a comparison between MATLAB and Adams Moulton Predictor-Corrector method (AMPC)

is shown in Figs. 2 and 3. The solid lines correspond to MATLAB BVP4C and the yellow dots to AMPC. Excellent correlation is achieved for each selected case benchmarked in each of the figures demonstrating the precision of the MATLAB method used for all renderings.

### 5. Numerical results and discussion

Extensive visualizations of the transport characteristics have been presented in Figs. 2-7. In all computations, the following default parameters are prescribed:

$C = 0.5, M = 0.5, \delta = 0.3, m = 0.2, \lambda = 0.3, Ec = 0.2, Pr = 1.0, Re_x = 0.2$ . These corresponds to physically realistic magnetic polymer and thermal characteristics [65,66].

Figs. 2(a-g) illustrate the evolution of primary velocity with transverse coordinates for various values of the non-Newtonian couple stress parameter ( $C$ ). As per the Stokes formulation, it is therefore associated with the highest order derivative term and will have a

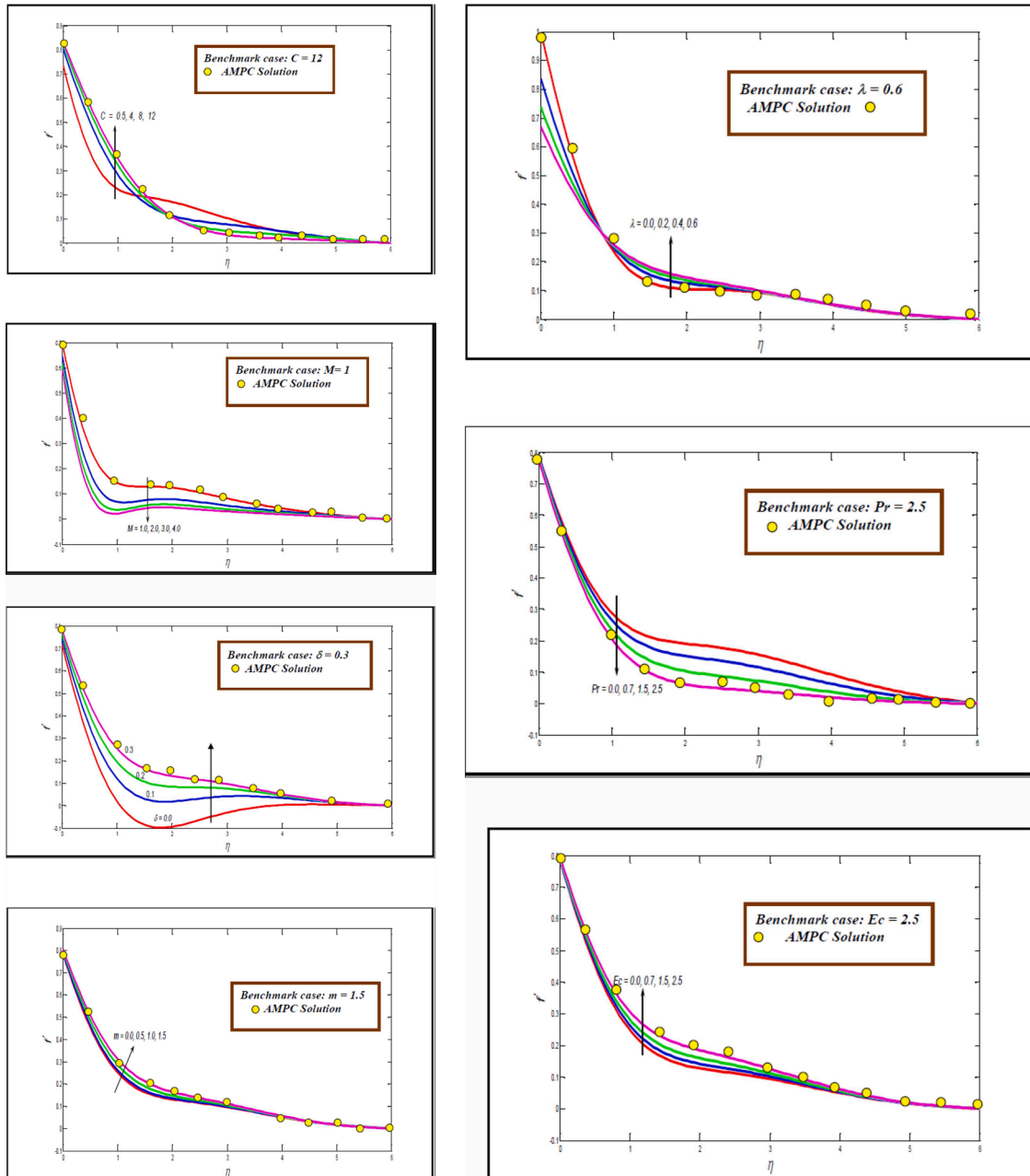


Fig. 2. Velocity plots for various (a)C, (b)  $M$ , (c)  $\delta$ , (d)  $m$ , (e) $\lambda$ , (f)  $Pr$  and (g)  $Ec$  ..

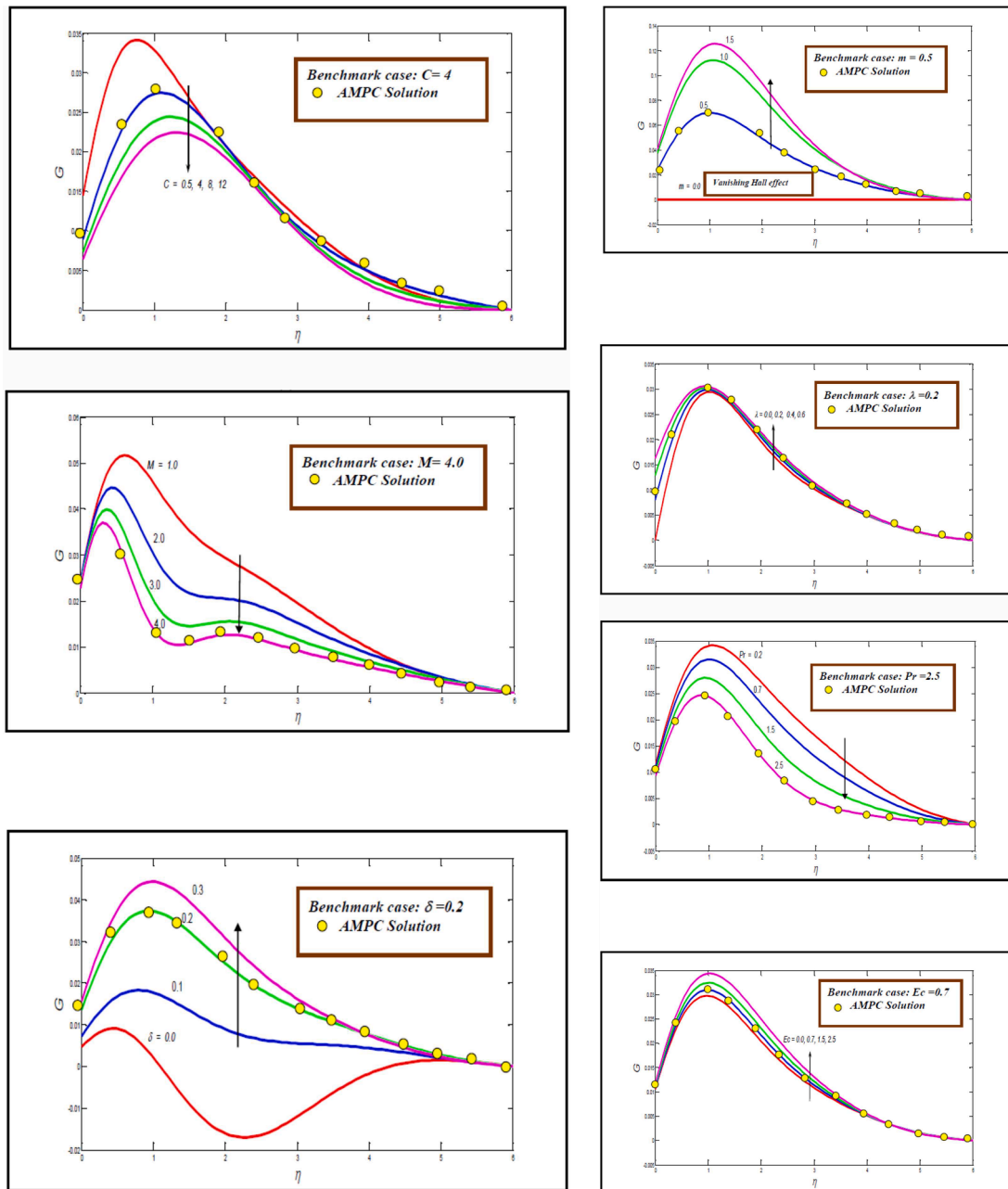


Fig. 3. Secondary velocity plots for various (a)C, (b) M, (c)  $\delta$ , (d) m, (e)  $\lambda$ , (f) Pr and (g)  $E_c$  ..

significant effect on momentum transfer. Increment in C values (Fig. 2a) strongly boost the primary velocity,  $f'(\eta)$  nearer the wall (substrate) indicating that couple stresses in the magnetic polymer accelerate the primary flow and thin the momentum boundary layer. However further from the wall, there is a reversal in this effect, and this is attributable to the relaxation in the fluid with greater space for the rigid elements. A similar observation has been made by Stokes [13] and others. Strong non-Newtonian behavior in terms of couple stresses is therefore beneficial to the primary flow. Fig 2b shows that elevation in magnetic interaction parameter (also known as the Stuart number which defines the ratio of the Lorentzian magnetic drag to the inertial force). The linear Lorentzian drag force inhibits velocity improvements and leads to a thinning in boundary layer thickness. This effect, unlike the couple stress effect, is sustained at all locations into the boundary layer regime transverse to the wall i. e. from the leading edge (origin point of the polymer thin shear layer growth on the wall) to the free stream. Reverse flow i.e. negative values never arise in the primary velocity indicating that the direction of the flow is never changed, irrespective of the strength of the magnetic field imposed. Fig. 2c reveals that increment in mixed convection parameter ( $\delta$ ) induces a strong acceleration in the primary flow. The forced convection case is retrieved with  $\delta = 0$

for which thermal buoyancy effects are negated. This leads to a minimization in primary velocity and a thicker momentum boundary layer. With a stronger mixed convection effect, thermal buoyancy forces are amplified which energizes the flow and reduces the hydrodynamic boundary layer thickness. The parameter,  $\delta$  features in the coupling term,  $-\delta\theta$  in the primary momentum Eqn. (14). When  $\delta \rightarrow 0$  the primary Eqn. (14) and energy eqn. (15) are decoupled (*forced convection case*). Despite being a *first-order linear term*, the mixed convection effect is substantial and significantly alters the velocity distribution as noted by Bejan [66]. Inevitably the exponential stretching rate will also contribute to the momentum transfer modification, as noted by Venkatadri et al. [67]. Fig. 2d illustrates that elevation in the Hall parameter ( $m$ ) markedly accelerates the primary flow and this response is sustained throughout the boundary layer. In Eqn. (14),  $m$  arises in the modified magnetohydrodynamic term  $+\frac{M}{(1+m^2)}(f' + m g)$  and appears both as a quadratic term in the denominator and a linear term in the numerator, coupled with the secondary velocity field in the latter ( $m g$ ). The dominant influence will be the linear term, as mentioned in Cramer and Pai [30] among others. Momentum will be boosted with a stronger Hall parameter via the cross-flow (secondary flow) effect, which will reduce the momentum boundary layer thickness. Since the primary flow is dampened by the traditional Lorentzian magnetic drag force, the Hall parameter produces the opposite effect (acceleration). Engineers therefore have the dual mechanism of both magnetic field and Hall parameter to generate both deceleration and acceleration in the coating regime and of course, there is a delicate interplay in practical operations as noted in Fink [65]. Fig. 2e demonstrates that with elevation in generalized slip effect,  $\lambda$ , the primary velocity is boosted.

The molecular slip in the vicinity of the boundary clearly aids in momentum development. However further into the boundary layer this effect decays away and vanishes in the free stream. Neglecting of hydrodynamic slip therefore under predicts the velocity in the near-wall region. The slip effect is of course simulated only via the augmented wall primary velocity boundary condition in Eqn. (17), viz  $f'(0) = 1 + \lambda f'(0)$ . This simple model however does capture the non-adherence reported in polymeric boundary layer flows and correctly simulates the observed behavior as reported in [53,54]. Fig. 2f shows that with higher Prandtl numbers there is a significant decrement in primary velocity. Magnetic polymers [65] have generally much lower Prandtl numbers than conventional polymers owing to the presence of metallic magnetic particles (which boost thermal conductivities). The overall effect is to inhibit momentum diffusion with a greater Prandtl number and induce a thinner  $f$ . Fig. 2g informs that elevation in Eckert number,  $Ec$ , produces a notable boost in primary velocity. The dissipation effect is simulated both in the classical viscous heating term and the Ohmic dissipation term, which appears respectively as  $+\frac{Pr Ec}{2}(f' + G')^2$  and  $+Pr Ec M((f')^2 + G^2)$  in the energy Eqn. (16). While the classical result is to induce deceleration [30] with greater destruction of kinetic energy via internal friction or magnetic drag, this is not experienced in magnetic polymers, as noted in Fink [65] and other studies. The primary flow is accelerated, and a similar effect will be induced in the secondary flow. The magnetic polymer experiences molecular relaxation with a greater dissipation effect and via elastic forces this encourages momentum diffusion leading to a thinner hydrodynamic boundary layer thickness (primary flow acceleration).

Figs. 3a-g visualize the secondary velocity ( $G$ ) response to increment in various  $C, M, \delta, m, \lambda, Pr$  and  $Ec$ . In some cases, similar trends are computed as for the primary velocity field, although there are major distinctions, especially in the near wall zone (close to the polymer sheet surface) and for the couple stress effect. Fig. 3a shows that a strong deceleration is induced in the secondary flow with a greater couple stress effect,  $C$ . The relevant term in the secondary momentum Eqn. (15),  $\frac{C Re_x}{4} g^{IV}$ , is inhibiting to secondary flow development in the near-wall regime (it is *assistive* for the primary flow case), but secondary flow is accelerated. These characterize the nature of the cross-flow in Hall current magnetohydrodynamics where a re-balance in primary and secondary momentum is known to occur, as noted in Cramer and Pai [44] and other studies [59,60,63]. Fig. 3b shows that with increasing Stuart number there is a significant reduction in  $G$ . However, the oscillatory nature of the flow which largely arises near the wall is not computed in the primary flow case, especially at high magnetic field strengths. This indicates the possible onset of instability in the regime, which can be avoided by tuning the magnetic field to be of intermediate strength ( $M \sim 2$ ). The net effect of magnetic parameter is to suppress momentum diffusion in the secondary flow and to increase hydrodynamic boundary layer thickness. Fig. 3c visualizes the impact of the mixed convection parameter,  $\delta$  on secondary velocity evolution. As with the primary momentum balance eqn. (14), the same term,  $-\delta\theta$  arises in the secondary momentum eqn. (15). Increasing  $\delta$  values mobilize thermal convection current with stronger thermal buoyancy in the regime. This accelerates the secondary flow and simultaneously eliminates the unstable periodic patterns encountered in the forced convection case ( $\delta = 0$ ) and weak mixed convection case ( $\delta = 0.1$ ). For larger  $\delta$ , the  $f$  is also improved.

Fig. 3d illustrates the response in secondary velocity to an increment in Hall parameter ( $m$ ). As with the primary flow field, a similar term arises for Hall effects in the secondary flow eqn. (15), although the coupling nature is different. In the latter, the coefficient is the same i.e.  $-\frac{M}{(1+m^2)}$  whereas the velocity term is ( $m = f' - G$ ). In the former (primary) however the velocity term is ( $f' + m G$ ). This produces a strong crossover in physics, with different manifestations in the velocity fields. While a weaker acceleration is induced in the primary flow with a greater Hall effect (higher  $m$  values), a much more dramatic elevation is encountered in the secondary flow. Backflow is absent in the primary flow at any location or Hall parameter value and the same is witnessed for the secondary flow. However, the vanishing Hall current case ( $m = 0$ ) produces no variation in secondary velocity whereas it does modify the primary velocity. A much thinner is also caused in the secondary flow compared with the primary flow and magnitudes of secondary velocity, as anticipated (due to the cross-flow nature of the Hall effect) are significantly larger than the primary flow velocities. The inclusion of Hall current in magnetic polymer coating boundary layer flows therefore produces a compensating effect (acceleration) for the retardation induced by the magnetic Lorentz body force effect (which is controlled by the Stuart number,  $M$ ). This provides a powerful dual methodology for modifying momentum characteristics (also influenced by deposition rates of magnetic particles embedded in polymers) in such applications as noted by Yang and Huang [68] among many others. Figs. 3e-g show that with increment in slip parameter ( $\lambda$ ), Prandtl number ( $Pr$ ) and Eckert (dissipation) number ( $Ec$ ), there is a respective enhancement, decrement and elevation in secondary flow velocities. The most dramatic modification is induced by Prandtl number and the weakest modification is produced

with a change in hydrodynamic wall slip. Therefore, the secondary flow overall shows less sensitivity to these three parameters compared with the primary flow distributions.

Figs. 4a-g display the temperature response to alterations in the values of  $C$ ,  $M$ ,  $\delta$ ,  $m$ ,  $\lambda$ ,  $Pr$  and  $Ec$ , respectively. Figs. 4a, b show, that increasing couple stress rheological effect depresses temperature whereas elevation in Stuart magnetic interaction number induces the opposite effect and elevates temperatures.. This heats the polymer boundary layer regime and elevates thermal boundary layer thicknesses. Temperatures are therefore minimal for least value of  $M = 1.0$  when the Lorentz and inertial forces are exactly balanced. These trends are sustained at all values of transverse coordinate and asymptotically smooth convergence is achieved in the free stream, again confirming the prescription of an adequately large infinity boundary condition in the MATLAB code. Figs 4c, d indicate that with increment in mixed convection parameter ( $\delta$ )and Hall parameter ( $m$ ) there is also a consistent suppression in temperatures. Thermal boundary layer thickness is therefore depleted with stronger thermal buoyancy and Hall current effect. The Hall parameter therefore exerts the opposite influence to the magnetic interaction (Stuart) number on temperature evolution i.e. it cools the electroconductive polymer boundary layer regime. Figs. 4e, f, g generally demonstrate that there is a weak increase, strong decrease and strong elevation,

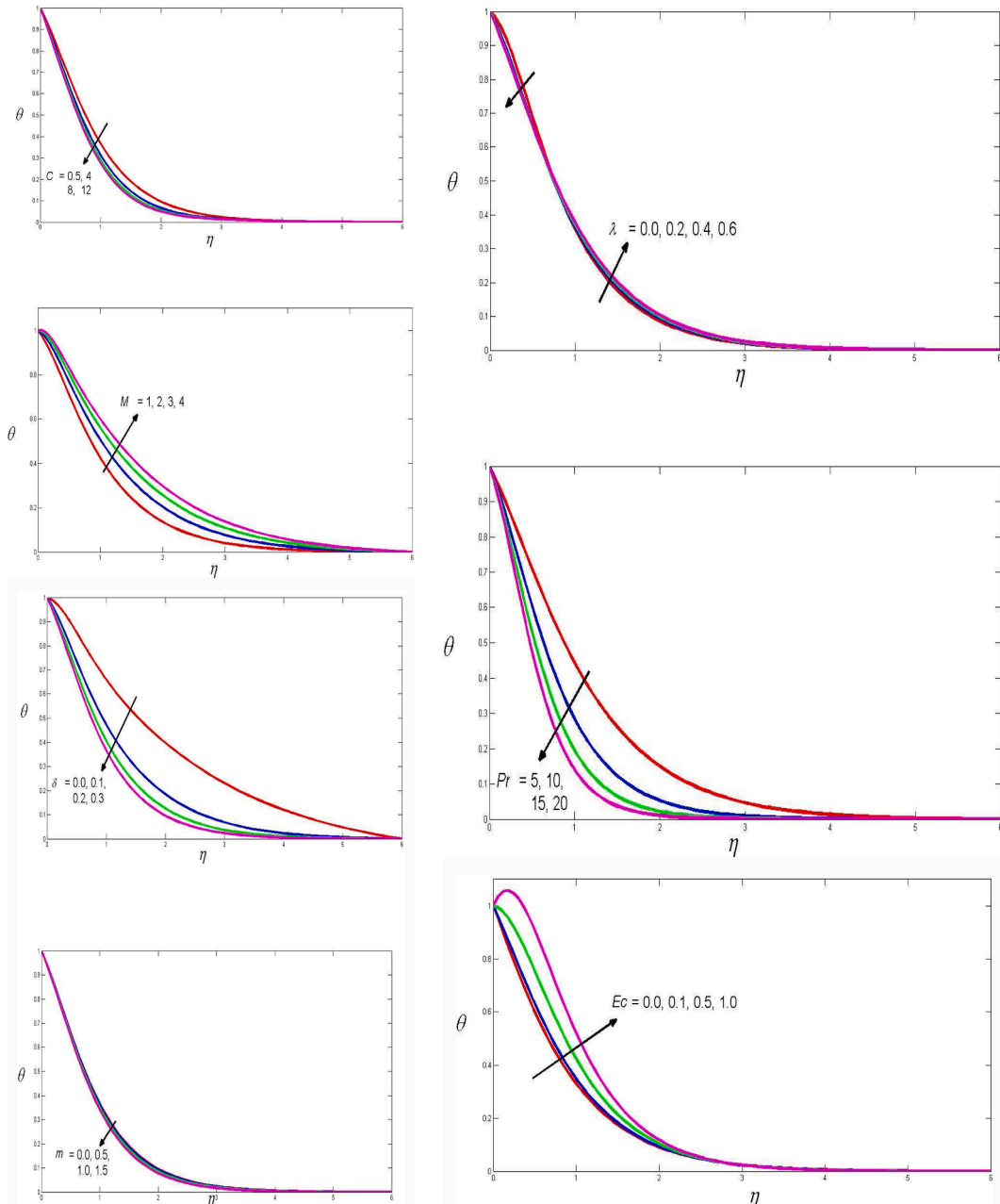


Fig. 4. Temperature distributions for various (a)C, (b)  $M$ , (c)  $\delta$ , (d)  $m$ , (e) $\lambda$ , (f)  $Pr$  and (g)  $Ec$  ..

respectively induced in temperatures with enhancement in hydrodynamic generalized slip effect, Prandtl number and Eckert number. The wall slip principally modifies the velocity field although via buoyancy coupling terms it indirectly effects the temperature. Higher Pr indicates to lower thermal conductivities of the magnetic polymer which in turn reduces thermal diffusion. This inhibits heat transfer and decreases temperatures. Increasing Eckert number on the other hand accentuates the mechanical energy converted to internal friction (thermal energy) and the kinetic energy dissipated by the action of the magnetic field (Joule heating magneto-calorific effect i. e. Ohmic dissipation) [65] which both manifest in an amplification in temperatures and thicker thermal boundary layers. These trends concur with a number of other studies on hydromagnetic polymer processing including Das et al. [59] (for exponential stretching). It is also interesting to note that at a low Prandtl number ( $Pr = 0.2$ ) there is an approximate linear temperature decay from the wall to the far stream whereas with higher  $Pr$  values the topology warps to a strongly parabolic nature. A temperature overshoot is also only computed in close proximity to the wall at the highest Eckert number- this overshoot vanishes at lower values i. e. weaker viscous and Ohmic dissipation.

Figs. 5-7 present the secondary skin friction ( $G' = C_{f_z}$ ), primary skin friction ( $f'' = C_{f_x}$ ), and local Nusselt number ( $Nu_x$ ). A slight decrease in secondary skin friction accompanies a large increment in magnetic interaction parameter,  $M$  (Fig. 5). This concurs with the damping in secondary velocity reported in earlier graphs and confirms the inhibiting nature of Lorentzian magnetic drag force which causes the boundary layer flow to shear more slowly along the substrate (wall). However as also computed earlier, a strong acceleration is observed with increasing Hall parameter ( $m$ ). As expected, a much stronger depreciation in primary skin friction is induced with increment in magnetic parameter,  $M$  (Fig. 6). Primary flow is therefore strongly retarded as computed earlier. This confirms the opposite effects of magnetic Lorentzian drag force and Hall currents which induce deceleration and acceleration respectively in the coating flow regime. A strong depletion in the Nusselt number is computed with increasing Stuart magnetic interaction parameter,  $M$ . This physically concurs with the strong elevation in temperatures computed earlier. Greater Lorentz force heats the boundary layer, and this exacerbates the transfer of heat from the wall to the bulk fluid and hence lowers the Nusselt numbers. An intensification in Hall current ( $m$ ) generates the opposite effect – it elevates Nusselt numbers since it is known to induce heating in the boundary layer resulting in a suppression in heat transfer to the wall.

### 6. Conclusions

As a simulation of electro-magnetic polymer coating flow on a horizontal substrate, viscous magnetohydrodynamic non-Newtonian boundary layer flow of an incompressible, electrically conducting, couple stress, electroconductive polymer from an exponentially stretching sheet has been studied in this paper. Owing to the slippery motion at the substrate, a slip velocity is included. A secondary flow is induced with the presence of a Hall current. Ohmic and viscous dissipations are also incorporated in the mathematical formulation. The nonlinear boundary value problem is solved by adopting the shooting technique and bvp4c algorithm available in MATLAB software. The simulations have shown that:

- (i) Increasing the magnetic interaction number, reduces the primary skin friction whereas it strongly depletes secondary skin friction and also the Nusselt number.

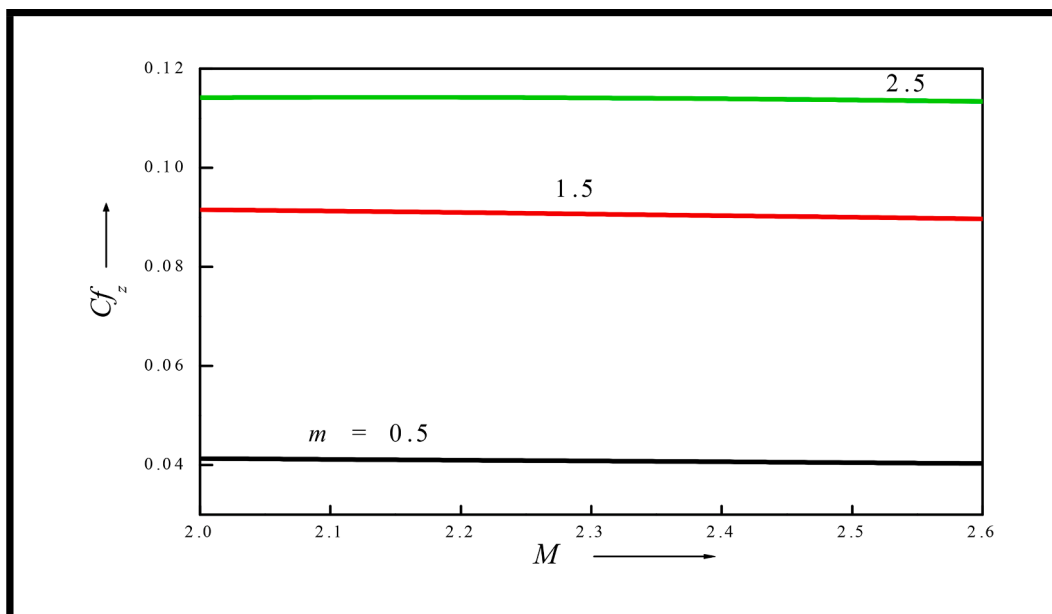


Fig. 5. Primary skin friction variation with Hall parameter ( $m$ ) and magnetic interaction (Stuart) number ( $M$ ) .

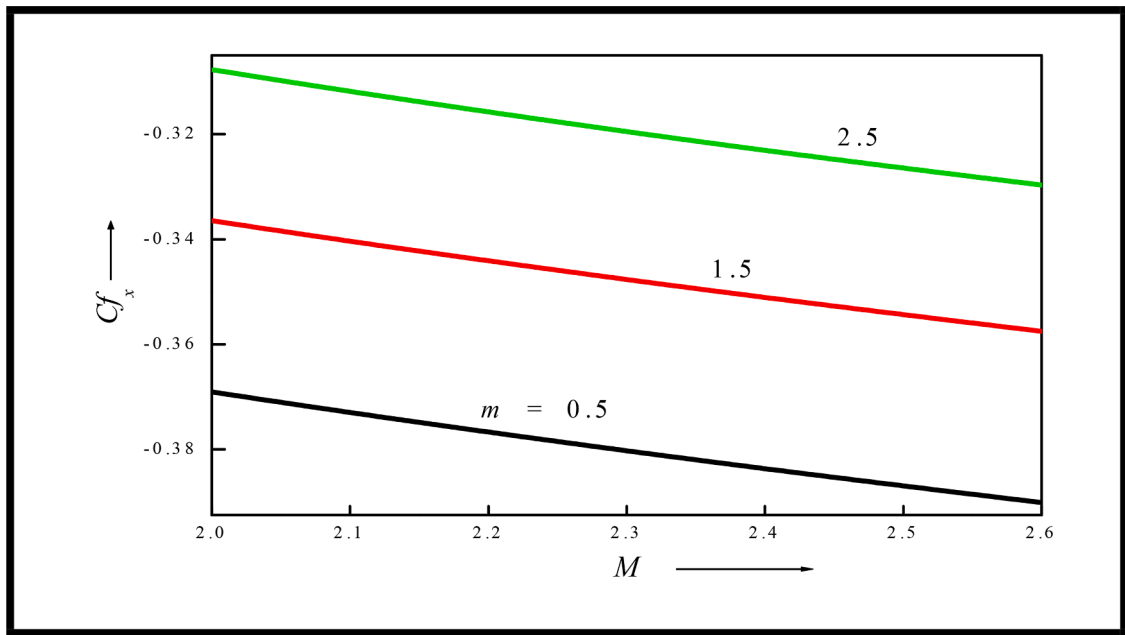


Fig. 6. Secondary skin friction variation with Hall parameter ( $m$ ) and magnetic interaction number ( $M$ ).

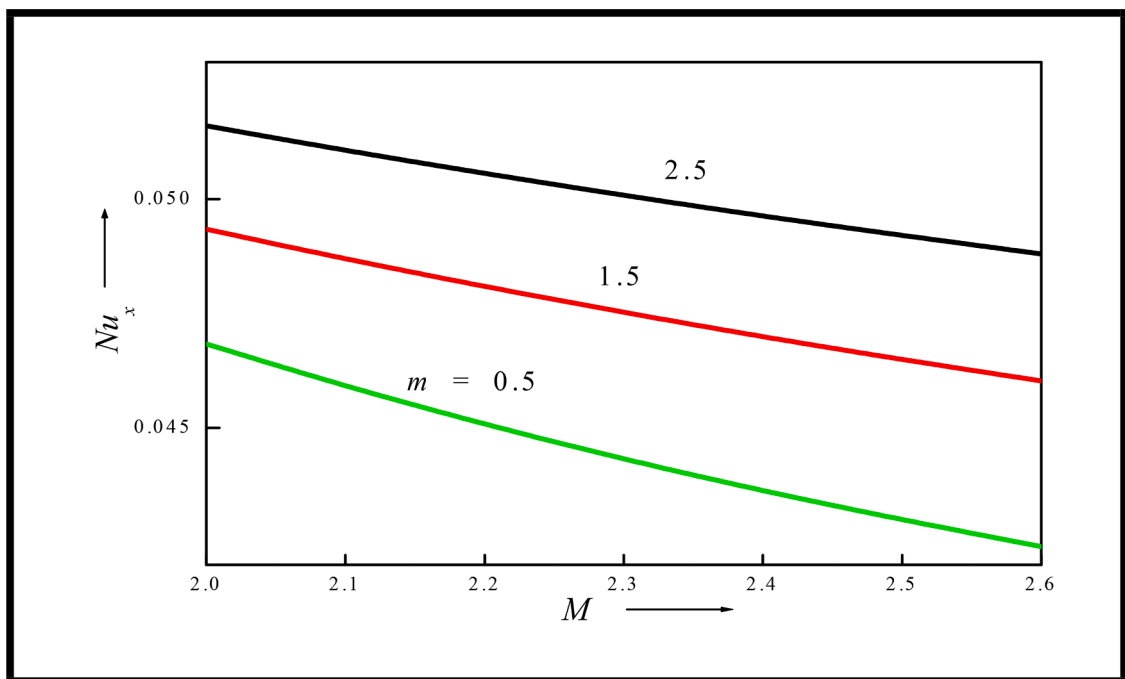


Fig. 7. Nusselt number variation with Hall parameter ( $m$ ) and magnetic interaction number ( $M$ ).

- (ii) Increasing Hall parameter significantly elevates both primary and secondary skin friction coefficients and also induces a boost in the local Nusselt number.
- (iii) Temperatures (and thermal boundary layer thicknesses) are boosted with Eckert number (a temperature overshoot accompanies the strongest case of viscous heating i. e.  $Ec = 2.5$ ) whereas they are significantly suppressed with increasing Hall parameter.
- (iv) Temperatures are also reduced with greater Prandtl number but slightly increased with higher values of generalized slip parameter.

- (v) With increasing magnetic interaction number there is a substantial elevation in the Ohmic heating effect and an associated increase in temperature and thermal boundary layer thickness.
- (vi) With the increment in mixed convection parameter and non-Newtonian couple stress parameter, there is a marked reduction in temperatures.
- (vii) An increase in Eckert number elevates both primary and secondary velocities whereas greater Prandtl number decelerates both the primary and secondary flow.
- (viii) Greater hydrodynamic slip effect initially boosts the primary velocity near the wall but thereafter induces a decrement in it. However, a consistent elevation in secondary velocity is computed with increasing slip parameter.
- (ix) Increasing the Hall parameter strongly accelerates the secondary flow but only weakly accelerates the primary flow.
- (x) Increasing magnetic interaction number decelerates the primary flow although back flow is never induced; secondary flow is however very significantly decelerated with greater magnetic interaction number i.e. stronger transverse magnetic field, and significant backflow is mobilized in the boundary layer regime.
- (xi) Elevation in mixed convection parameter notably accelerates and stabilizes the secondary flow and also generates significant primary flow acceleration.
- (xii) Higher values of coupled stress parameter initially accelerate the primary flow near the substrate (wall) whereas deeper into the boundary layer transverse to the wall it induces a deceleration into the free stream. Secondary flow is however consistently decelerated throughout the boundary layer with stronger non-Newtonian couple stress effects.

The present study has shown that both MAPLE bvp4c and Adams-Moulton predictor corrector methods are excellent numerical methods for simulating nonlinear magnetic functional polymer coating flows. Attention has however been confined to steady-state flows. Future endeavors may address *time-dependent* effects and will be communicated imminently.

### Declaration of Competing Interest

The authors declare that they have no known competing financial interests or personal relationships that could have appeared to influence the work reported in this paper.

### Acknowledgement

MS acknowledge the financial support from University of Technology and Applied Sciences, Ibri, Oman under the Internal Research Funding via Project Number: DSRIRPS-2021–22-PROP-1.

### References

- [1] Y. Zhang, Q. Wang, S. Yi, Z. Lin, C. Wang, Z. Chen, L. Jiang, 4D Printing of magnetoactive soft materials for on-demand magnetic actuation transformation, *ACS Appl. Mater. Interfaces* 13 (3) (2021) 4174–4184.
- [2] R. Xiao, W.M. Huang, Heating/solvent responsive shape-memory polymers for implant biomedical devices in minimally invasive surgery: current status and challenge, *Macromol. Biosci.* 20 (8) (2020), e2000108.
- [3] Q. Ze, et al., Magnetic Shape memory polymers with integrated multifunctional shape manipulation, *Adv. Mater.* 32 (4) (2020), 1906657.
- [4] Y. Xia, Y. He, F. Zhang, Y. Liu, J. Leng, A review of shape memory polymers and composites: mechanisms, materials, and applications, *Adv. Mater.* 33 (6) (2020) 119–126, 6.
- [5] T. Wang, et al., Electroactive polymers for sensing, *Inter. Focus* 6 (4) (2016) 1–19.
- [6] A.J. Lovinger, Ferroelectric polymers, *Science* 220 (4602) (1983) 1115–1121.
- [7] K.J. Kim, S. Tadokoro, *Electroactive Polymers for Robotic Applications, Artificial Muscles and Sensors*, Springer, London, 2007.
- [8] R.B. Bird, R.C. Armstrong, *Dynamics of Polymeric Liquids*, 2nd edition, John Wiley & Sons, New York, NY, USA, 1987 vol. 1.
- [9] M.T. Shaw, *Introduction to Polymer Rheology*, Wiley, New York, NY, USA, 2012.
- [10] A.C. Eringen, *Microcontinuum Field Theories*, Springer, New York, 2001.
- [11] A.C. Eringen, Theory of micropolar fluids, *J Math Mech* 16 (1966) 1–18.
- [12] A.C. Eringen, Micropolar fluids with stretch, *Int. J. Engineering Science* 7 (1) (1969) 115–127.
- [13] V.K. Stokes, Couple stresses in fluid, *Phys. Fluids* 9 (1966) 1709–1715.
- [14] V.K. Stokes, *Theories of Fluids with Microstructure: An Introduction*, Springer Verlag, New York, USA, 1984.
- [15] S.C. Cowin, The theory of polar fluids, *Adv. Appl. Mech.* 14 (1974) 279–347.
- [16] U.M. Mokhiamer, W.A. Crosby, H.A. El-Gamal, A study of a journal bearing lubricated by fluids with couple stress considering the elasticity of the liner, *Wear* 224 (1999) 194–201.
- [17] M. Devakar, D. Sreenivasu, B. Shankar, Analytical solutions of couple stress fluid flow with slip boundary conditions, *Alex. Eng. J.* 53 (2014) 723–730.
- [18] M. Devakar, T.K.V. Iyengar, Run up flow of a couple stress fluid between parallel plates, *Non-Linear Anal.* 15 (2010) 29–37.
- [19] S. Islam, I. Ali, A. Shah, X.J. Ran, A.M. Siddiqui, Effect of couple stresses on flow of third grade fluid between two parallel plates using homotopy perturbation method, *Int. J. Nonlinear Sci. Numer. Simul.* 10 (2009) 99–112.
- [20] M. Farooq, M.T. Rahim, S. Islam, A.M. Siddiqui, Steady Poiseuille flow and heat transfer of couple stress fluids between two parallel inclined plates with variable viscosity, *J. Assoc. Arab Univ. Basic Appl. Sci.* 14 (2013) 9–18.
- [21] V.M. Soundalgekar, Effects of couple stress in fluids on dispersion of a solute in a channel flow, *Phys. Fluids* 14 (1971) 19–20.
- [22] J. Zueeo, O.A. Beg, Network Numerical simulation applied to pulsatile non-newtonian flow through a channel with couple stress and wall mass flux effects, *Int. J. Appl. Math. Mech.* 5 (2) (2009) 1–16.
- [23] J.C. Umavathi, M.S. Malashetty, Oberbeck convection flow of a couple stress fluid through a vertical porous stratum, *Int. J. Non Linear Mech.* 34 (1999) 1037–1045.
- [24] D. Srinivasacharya, D. Srikanth, Effect of couple stresses on the flow in a constricted annulus, *Arch. Appl. Mech* 78 (2008) 251–257.
- [25] A. Ogulu, On the oscillating plate-temperature flow of a polar fluid past a vertical porous plate in the presence of couple stresses and radiation, *Int. Comm. Heat Mass Trans.* 32 (2003) 1231–1243.

- [26] M.S. Malshetty, J.C. Umavathi, Oberbeck convection flow of a couple stress fluid through a vertical porous stratum, *Int. J. Non-Linear Mech.* 34 (1999) 1037–1045.
- [27] J.C. Umavathi, A.J. Chamkha, M.H. Manjula, A. Al-Mudhaf, Flow and heat transfer of a couple-stress fluid sandwiched between viscous fluid layers, *Canadian J. Phys.* 83 (2005) 705–720.
- [28] M. Kumar, G.J. Reddy, N.N. Kumar, O.Anwar Bég, Application of differential transform method to unsteady free convective heat transfer of a couple stress fluid over a stretching sheet, *Heat Trans.* (2018), 19 pages.
- [29] J.C. Umavathi, O.Anwar Bég, Modelling the onset of thermosolutal convective instability in a non-Newtonian nanofluid-saturated porous medium layer, *Chinese J. Phys.* 68 (2020) 147–167.
- [30] A.U. Awan, R. Safdar, M. Imran, A. Shaukat, Effects of chemical reaction on the unsteady flow of an incompressible fluid over a vertical oscillating plate, *Punjab University J. Mathem.* 48 (2016) 167–182.
- [31] A.U. Awan, M. Imran, M. Athar, M. Kamran, Exact analytical solutions for a longitudinal flow of a fractional maxwell fluid between two coaxial cylinders, *Punjab University J. Mathem.* 45 (2013) 9–23.
- [32] A.U. Awan, et al., Significance of magnetic field and Darcy–Forchheimer law on dynamics of Casson-Sutterby nanofluid subject to a stretching circular cylinder, *Int. Comm. In Heat Mass Trans.* 139 (2022), 106399.
- [33] Insight into the heat transfer of thirdgrade micropolar fluid over an exponentially stretched surface, *Sci. Rep.* 12 (2022) 15577.
- [34] Dynamics of rotating micropolar fluid over a stretch surface: the case of linear and quadratic convection significance in thermal management, *Nanomaterials* 12 (2022) 3100.
- [35] A.U. Awan, S. Riaz, S. Sattar, K.A. Abro, Fractional modeling and synchronization of ferrofluid on free convection flow with magnetolysis, *Europ. Phy. J. Plus* 135 (2020) 841–855.
- [36] A.U. Awan, M. Aziz, N. Ullah, S. Nadeem, K.A. Abro, Thermal analysis of oblique stagnation point flow with slippage on secondorder fluid, *J. Thermal Analy. Calorim.* 147 (2022) 3839–3851.
- [37] Q. Ali, S. Riaz, A.U. Awan, Free convection MHD flow of viscous fluid by means of damped shear and thermal flux in a vertical circular tube, *Physica Scripta* 95 (2020), 095212.
- [38] A.U. Awan, et al., Numerical analysis of heat transfer in Ellis hybrid nanofluid flow subject to a stretching cylinder, *Case Stud. Thermal Engin.* 49 (2023), 103222.
- [39] M.A. Shahzad, et al., On the steady flow of non-newtonian fluid through multi-stenosed elliptical artery: a theoretical model, *Ain. Shams. Engin. J.* (2023), <https://doi.org/10.1016/j.asej.2023.102262>.
- [40] N. Abbas, K.U. Rehman, W. Shatanawi, K. Abodayeh, Mathematical model of temperature-dependent flow of power-law nanofluid over a variable stretching Riga sheet, *Waves Random Compl. Media* (2023), <https://doi.org/10.1080/17455030.2022.2111029>.
- [41] T.A.M. Shatanawi, N. Abbas, W. Shatanawi, Comparative study of Casson hybrid nanofluid models with induced magnetic radiative flow over a vertical permeable exponentially stretching sheet, *AIMS Mathem.* 7 (2022) 20545–20564.
- [42] A.A.M. Shatanawi, N. Abbas, W. Shatanawi, Mathematical analysis of unsteady stagnation point flow of radiative Casson hybrid nanofluid flow over a vertical Riga sheet, *Mathematics* 10 (2022) 3573–3590.
- [43] O.Anwar Bég, S.K. Ghosh, T.A. Bég, *Applied Magnetofluid Dynamics- Modelling and Computation*, Lambert Academic, Germany, 2011, 411pp.
- [44] K.C. Cramer, S.I. Pai, *Magnetofluid Dynamics for Engineers and Applied Physicists*, MacGraw-Hill, New York, USA, 1973.
- [45] L.J. Crane, Flow past a stretching plate, *ZAMP* 21 (1970) 645–650.
- [46] N.S. Akbar, D. Tripathi, O.Anwar Bég Z.Khan, A numerical study of magnetohydrodynamic transport of nanofluids from a vertical stretching sheet with exponential temperature-dependent viscosity and buoyancy effects, *Chem. Phys. Lett.* 661 (2016) 20–30.
- [47] G.N. Sekhar, A.S. Chethan, Flow and heat transfer of quadratic stretching sheet in a Boussinesq-Stokes' suspension, *Int. J. Appl. Mech. Engin.* 16 (4) (2010) 1109–1128.
- [48] [37] R. Bhargava, S. Sharma, H.S. Takhar, O. Anwar Bég, P. Bhargava, Numerical solutions for micropolar transport phenomena over a nonlinear stretching sheet, *Model. Control J* 12 (1) (2007) 45–63.
- [49] B. Bidin, R. Nazar, Numerical solution of the boundary layer flow over an exponentially stretching sheet with thermal radiation, *Europ. J. Scient. Res.* 33 (4) (2009) 710–717.
- [50] A. Nayak, G.C. Dash, Magnetohydrodynamic couple stress fluid flow through a porous medium in a rotating channel, *J. Engin. Thermophys.* 24 (2015) 283–295.
- [51] K. Ramesh, M. Devakar, Effects of heat and mass transfer on the peristaltic transport of MHD couple stress fluid through porous medium in a vertical asymmetric channel, *J. Fluids* (2015). ID 163832 19 pages.
- [52] J.M. Piau, N.E. Kissi, Measurement and modelling of friction in polymer melts during macroscopic slip at the wall, *J. Non-Newtonian Fluid Mech.* 54 (1994) 121–142.
- [53] J.-M. Piau, N.E. Kissi, F. Toussaint, A. Mezghani, Distortions of polymer extrudates and their elimination using slippery surfaces, *Rheol. Acta.* 34 (1995) 40–57.
- [54] S.Q. Wang, P.A. Drda, Y.W. Inn, Exploring molecular origins of sharkskin, partial slip, and slope change in flow curves of linear low-density polyethylene, *J. Rheol.* 40 (5) (1996) 875–898.
- [55] M.M. Bhatti, C.M. Khaliq, T. Bég, O.Anwar Bég, Ali Kadir, Numerical study of slip and radiative effects on magnetic Fe<sub>3</sub>O<sub>4</sub>-water-based nanofluid flow from a nonlinear stretching sheet in porous media with Soret and Dufour diffusion, *Modern Phys. Lett. B* 33 (2020), 2050026, 24 pages.
- [56] O.Anwar Bég, J. Zueco, L.M. López-Ochoa, Network numerical analysis of optically thick hydromagnetic slip flow from a porous spinning disk with radiation flux, variable thermophysical properties and surface injection effects, *Chem. Eng. Commun.* 198 (3) (2011) 360–384.
- [57] S.R. Mishra, M.D. Shamsuddin, O. Anwar Bég, A. Kadir, Viscous dissipation and Joule heating effects in non-Fourier MHD squeezing flow, heat and mass transfer between Riga plates with thermal radiation: variational parameter method solutions, *Arab. J. Sci. Engin.* (2019), 15 pages.
- [58] M. Kumar, G.J. Reddy, N.N. Kumar, O.Anwar Bég, Computational study of unsteady couple stress magnetic nanofluid flow from a stretching sheet with Ohmic dissipation, *Proc. IMechE-Part N: J Nanoengineering, Nanomaterials and Nano-systems* (2019) (15 pages).
- [59] S. Das, R.R. Patra, R.N. Jana, The layout of Boussinesq couple-stress fluid flow over an exponentially stretching sheet with slip in porous space subject to a variable magnetic field, *Multidis. Model. Mater. Struc.* 16 (2020) 1131–1154.
- [60] M.D. Shamsuddin, S.U. Khan, O.A. Bég, T.A. Bég, Hall current, viscous and Joule heating effects on steady radiative 2-D magneto-power-law polymer dynamics from an exponentially stretching sheet with power-law slip velocity: a numerical study, *Thermal Sci. Engin. Progress* 20 (2020), 100732.
- [61] M.M. Bhatti, C.M. Khaliq, O.Anwar Bég, Ali Kadir, Differential transform solution for Hall and Ion slip effects on radiative-convective viscoplastic Casson flow from a stretching sheet with convective heating, *Heat Trans.* (2019), 17 pages.
- [62] O.Anwar Bég, Numerical methods for multi-physical magnetohydrodynamics, *J. Magnetohydrodynam. Plasma Res.* 18 (2) (2013) 93–200.
- [63] O.Anwar Bég, S.K. Ghosh, T.A. Bég, *Applied Magnetofluid Dynamics: Modelling and Computation*, Lambert Press, Germany, 2011.
- [64] S. Pal, *Numerical Methods: Principles, Analyses and Algorithms*, Oxford University Press, India, 2009.
- [65] J.K. Fink, *Metallized and Magnetic Polymers*, John Wiley & Sons, 2016.
- [66] A. Bejan, *Convection Heat Transfer*, Wiley, New York, 1984.
- [67] K. Venkatadri, S.A. Gaffar, V.R. Prasad, B. Md. H. Khan, O. Anwar Bég, Melting heat transfer analysis of electrically conducting nanofluid flow over an exponentially shrinking/stretching porous sheet with radiative heat flux under magnetic field, *Heat Trans.* 49 (8) (2020) 4281–4303.
- [68] Y.S. Yang, W. Huang, Magnetic field effects on coating deposition rate and surface morphology coatings using magnetron sputtering, *Smart Mater. Struct.* 19 (2010), 124003.